Weakened ~~and Irregular~~ Miocene Temperature~~Climate~~ Response to Orbital Forcing compared to the modern day

Yurui Zhang[1*], Jilin Wei[2,3], Zhen Li[1], Nan Dai[1], Weipeng Zheng[2,3,4] , Qiuzhen Yin[5], Agatha M. de Boer[6], Zhengguo Shi[7,8], Lixia Zhang[2]

[1]State Key Laboratory of Marine Environmental Science, College of Ocean & Earth Sciences, Xiamen University, Xiamen, China

[2]State Key Laboratory of Earth System Numerical Modeling and Application, Institute of Atmospheric Physics, Chinese Academy of Sciences, Beijing, China

[3]College of Earth and Planetary Sciences, University of Chinese Academy of Sciences, Beijing, China

[4]Earth System Numerical Simulation Science Center, Institute of Atmospheric Physics, Chinese Academy of Sciences, Beijing, China

[5]Earth and Climate Research Center, Earth and Life Institute, Universit écatholique de Louvain, Louvain-la-Neuve, Belgium

[6]Department of Geological Sciences, Bolin Centre for Climate Research, Stockholm University, Sweden

[7]State Key Laboratory of Loess Science, Institute of Earth Environment, Chinese Academy of Sciences, Xi'an, China

[8]Institute of Global Environmental Change, Xi'an Jiaotong University, Xi'an, China

Correspondence to: Yurui Zhang (yuruizhang@xmu.edu.cn)

Abstract. Although ~~O~~orbital forcing is pervasive in Miocene proxy records, the climate mechanisms linking insolation changes to regional temperature within this warm, low-ice climate state remains unclear~~a well-established driver of Pleistocene glacial-interglacial cycles, but its role in warmer climates remains less clear~~. Here we use fully coupled~~Using~~ climate model simulations to~~, we~~ assess temperature response to maximum and minimum boreal summer insolation under ~~during the~~ Miocene and pre-industrial (PI) conditions~~time~~. Both exhibit broadly anti-phased responses to increased and descreased insolation, but the Miocene response is~~shows~~ overall weaker, with regionally dependent contrasts and reduced symmetry ~~and less coherent~~ systematic between two orbital cases~~patterns~~. Three notable Miocene-PI differences emerge: (1) reduce ~~B~~boreal continental~~land~~ sensitivity~~regions respond less strongly~~ in the Miocene due to dampened albedo~~ feedbacks~~, water-vapor and cloud feedbacks in a warmer, low-~~ ~~ice climate~~from altered vegetation~~; (2) stronger Miocene cooling over tropical North Africa under high insolation, driven by intensified hydrological and moisture-feedbacks supported by a wider Tethys Sea~~Tropical Africa experiences stronger cooling under high insolation, driven by an intensified hydrological cycle with a broader Tethys Ocean under warm climate~~; (3) reversed~~The~~ Southern Ocean anomalies~~warms unexpectedly~~ under low insolation, where poleward-restricted Miocene~~linked to~~ sea ice ~~involved albedo feedbac~~enables winter insolation changes to trigger positive ice-albedo feedbacks~~k~~. These results demonstrate that background climate state strongly modulates orbital-scale responses and provide important context for interpreting Miocene proxy records and long-term changes in Earth's climate sensitivity through the Neogene. ~~Lower internal temperature variability in the Miocene suggests enhanced climate~~

~~stability and weaker orbital pacing. These findings highlight the importance of background climate state in shaping orbital-scale climate and interpreting proxy records.~~

1 Introduction

The Miocene (~23 to 5.3 Ma) marks~~was~~ a pivotal stage~~warm interval within~~ Earth's ~~the~~ long-term Cenozoic cooling trajectory~~end,~~ characterized by major reorganization of cryosphere, monsoon systems and global climate (Steinthorsdottir et al., 2021). The warmest interval of this epoch, the Miocene Climatic Optimum (MCO, ~17–14 Ma), was marked by globally elevated temperatures, reduced meridional temperature gradients, limited Antarctic sea ice, and intensified hydrological activity in the tropics and subtropics (Holbourn et al., 2013; Steinthorsdottir et al., 2021). Following the MCO, the climate transitioned toward cooler conditions, accompanied~~marked~~ by- stepwise expansion of Antarctic sea ice and intensified monsoons circulation (e.g., (Steinthorsdottir et al., 2021; Holbourn et al., 2013; Holbourn et al., 2018; Westerhold et al., 2020). These large-scale reorganizations have been widely interpreted as responses to changes in external forcing acting on an evolving climate background state.

A growing body of evidence links these Miocene climate changes to orbital forcing.~~These climatic changes have been linked to orbital forcing, notably~~ through mechanisms ~~such as~~involving Antarctic ice-sheet dynamics (Levy et al., 2019; Naish et al., 2009) and eccentricity-paced variations in the marine carbon cycle associated with an intensified tropical hydrological cycle (Holbourn et al., 2007; Liu et al., 2024; Tian et al., 2013). Long-term marine records further indicate that the sensitivity of Antarctic ice sheets to obliquity forcing intensified from ~~during~~ the Miocene onward and persisted~~continued~~ into~~to strengthen through~~ the Pliocene and Pleistocene (Levy et al., 2019; Van Peer et al., 2024). ~~In addition, s~~Spectral analyses of benthic $\delta^{18}O$ and $\delta^{13}C$ ~~proxies~~ records show~~indicate~~ dominatant 400 kyr eccentricity -pac~~ing~~ed ~~variability~~ during the Miocene, followed by the emergence of ~~with a subsequent transition toward~~ stronger 100 kyr and 40 kyr variability later in the Neogene ~~cycles~~ [*Holbourn et al.*, 2007; *Tian et al., 2013; Westerhold et al.*, 2020; *Liu et al., 2024*]. ~~Despite these insights, the underlying mechanism remains poorly understood due to a lack of targeted climate modelling studies.~~

~~It has been widely accepted that orbital forcing was at the origin of the Pleistocene glacial-interglacial cycles. A strong evidence is the good correlation between the periodicities of paleoclimate records and those of the astronomical parameters [Hays et al., 1976; Berger, 1978; *Lisiecki and Raymo*, 2005]. Earth's o~~Orbital variation in~~parameters —~~ eccentricity, obliquity, and precession —regulate the seasonal and latitudinal ~~timing and intensity of climate variability by altering the seasonal and spatial~~ distribution of incoming solar radiation, thereby influencing monsoon strength, cryosphere dynamics, and ocean–atmosphere coupling (Berger, 1978; Hays et al., 1976; Milanković, 1941~~69~~). Specifically, ~~S~~summer insolation in the high latitudes of the Northern Hemisphere (NH) has been suggested as a key driver of~~to control the~~ Quaternary glacial-interglacial cycle through ice–albedo and hydrological~~climate~~ feedbacks (Milanković, 1941; Berger, 1978~~69~~). Elevated NH summer insolation enhances land-sea thermal contrast, shifts convection inland, strengths ~~warms high-latitudes and enhances~~ rainfall ~~across regions~~

域代码已更改

域代码已更改

域代码已更改

域代码已更改

from Africa to Southeast Asia ~~by strengthening early-summer land heating and shifting convection inland~~ (Battisti et al., 2014; Bosmans et al., 2018; Dai et al., 2024; Herold et al., 2012; Yin et al., 2012). In the Southern Hemisphere, orbital forcing modulates Antarctic ice-sheet sensitivity, with geological records indicating enhanced obliquity responses from the Miocene onwards (Levy et al., 2019; Naish et al., 2009; Van Peer et al., 2024). Eccentricity-paced variations in the marine carbon cycle and tropical hydrological processes further point to a strong imprint of long-period orbital forcing during this interval (Holbourn et al., 2007; Tian et al., 2013; Liu et al., 2024).~~It has been widely accepted that orbital forcing was at the origin of the Pleistocene glacial-interglacial cycles. A strong evidence is the good correlation between the periodicities of paleoclimate records and those of the astronomical parameters [Hays et al., 1976; Berger, 1978; *Lisiecki and Raymo*, 2005].~~

However, the ~~Despite being a key external forcing~~ climate expression of orbital forcing is not stationary through time. Miocene $\delta^{18}O$ and $\delta^{13}C$ records are dominated by 400 kyr eccentricity variability, whereas stronger 100 kyr and 40 kyr cycles emerge later in the Neogene (Holbourn et al., 2007; Westerhold et al., 2020). ~~of the climate system, to which extent orbital forcing alone could explain the change of the dominant periodicity of glacial-interglacial cycle over the geological history remains uncertain. For instance,~~Comparable shifts ~~the dominant periodicity shifted from ~40 kyr to ~100 kyr over~~ during the Mid-Pleistocene transition (MPT) and the Mid-Brunhes Transition (MBT) occurred without major changes in orbital parameters, suggestiong an important role for background climate state, threshold behavior, or internal feedbacks related to the Southern Ocean ventilation and Antarctic ice dynamics~~the amplitude of the 100 kyr variability increased over the Mid-Brunhes Transition (MBT), but there are no strong obvious differences in the orbital parameters before and after these transitions (Berger, 1978;~~ (Laskar, 2010~~;). Orbitally-driven internal climatic processes have therefore been proposed to explain these transitions, such as a meridional shift in the Southern Hemisphere westerlies~~ (Kemp et al., 2010~~;) and changes in Southern Ocean ventilation and Antarctic bottom water formation (~~;Yin, 2013). Recent analyses further emphasize changes in the relative influence of precession and obliquity across these transitions~~N~~otably, a recent study found that the MBT coincides with a change of the relative importance of precession and obliquity on high-latitude insolation, while the MPT aligns with a weakening of both precession and obliquity variations, suggesting a potential orbital origin of these climate transitions~~ (Berger et al., 2024). Collectively, these observation imply a state-dependent orbital–climate relationship rather than a simple linear response to insolation forcing. ~~Furthermore, orbital variations can drive biome shifts, such as transitions from shrubland to tropical forest linked to Inter-Tropical Convergence Zone (ITCZ) variability, which may increase climate sensitivity to orbital forcing—as seen across the Eocene-Oligocene transition (Tardif et al., 2021; Westerhold et al., 2020). These studies highlight that the relationship between orbital forcing and climate is not constant in time, possibly due to internal climate feedbacks, boundary conditions and background climate.~~

Although geological archives document pervasive orbital pacing during the Miocene, the mechanisms by which orbital-scale insolation variations translate into regional climate responses—particularly in warm climates lacking large Northern Hemisphere ice sheets—remain poorly constrained. Proxy records alone cannot isolate the respective

roles of forcing, feedbacks, and internal variability, and climate modeling studies explicity targerting orbital effects under realistic Miocene boundary conditions remain scarce.

~~The Miocene (~23 to 5.3 Ma) was a warm interval within the long-term Cenozoic cooling trend, marked by stepwise expansion of Antarctic sea ice and intensified monsoons circulation (e.g., (Steinthorsdottir et al., 2021; Holbourn et al., 2013; Holbourn et al., 2018; Westerhold et al., 2020). These climatic changes have been linked to orbital forcing, notably through mechanisms such as Antarctic ice dynamics (Levy et al., 2019; Naish et al., 2009) and eccentricity-paced variations in the marine carbon cycle associated with an intensified tropical hydrological cycle (Holbourn et al., 2007; Liu et al., 2024; Tian et al., 2013). Long-term marine records indicate that the sensitivity of Antarctic ice sheets to obliquity forcing intensified during the Miocene and continued to strengthen through the Pliocene and Pleistocene (Levy et al., 2019; Van Peer et al., 2024). In addition, spectral analyses of $\delta^{18}O$ and $\delta^{13}C$ proxies indicate dominatant 400 kyr eccentricity-paced variability during the Miocene, with a subsequent transition toward stronger 100 kyr and 40 kyr cycles [*Holbourn et al.*, 2007; *Tian et al., 2013; Westerhold et al.*, 2020; *Liu et al., 2024*]. Despite these insights, the underlying mechanism remains poorly understood due to a lack of targeted climate modelling studies.~~

Here, we use fully coupled ~~By conducting~~ climate model simulations to ~~, this study~~ evaluate the climate response to orbital-driven insolation changes in ~~examines how~~ the Miocene framework.~~climate~~ We assess the sensitivity of high-latitude climate, tropical hydrological cycle~~responds to orbital~~, and ocean-cryosphere interactions to orbital forcing, and how these responses differ from those under the pre-industrial (PI) condition. By comparing these response with those patterns inferred from proxy records ~~forcing compared to the pre-industrial (PI) period, providing insight into~~ , we assess how background climate state modulates orbital-scale ~~climate feedback operates under different climate states (Steinthorsdottir et al., 2021). In particular, it explores how the absence of NH ice sheets, expanding Southern Ocean sea ice and strengthening monsoon rainfall shape Miocene orbital-scale~~ climate variability and to provide context for evaluation of orbital-climate coupling through the Neogene ~~on orbital scale~~.

2 Climate model and simulation setup

2.1 FGOALS-g3 climate model and simulation setup

We use the fully coupled general circulation model ~~-~~FGOALS-g3, which is part of CMIP6~~, to perform the simulations~~. It has been widely applied to both present-day climate studies (Li et al., 2020; Lin et al., 2022; Wang et al., 2020) and paleoclimate ~~studies~~ simulations from the Miocene to the mid-Holocene (Wei et al., 2023; Zheng et al., 2020). A ~~D~~detailed descripitions of model components and evaluation ~~about the model are~~ is provided in the Supplement~~ary information~~.

Two baseline experiments were conducted: a pre-industrial (PI) simulation and a Miocene simulation (MCO~~I 3x~~). The PI simulation i~~was~~ performed with standard~~with~~ pre-industrial climate forcing. The MCO~~I 3x~~ simulation adopts~~follows~~ the MioMIP2 protocol~~,~~ and incorporates ~~the~~ reconstructed Miocene boundary conditions, including

paleogeography, vegetation, ice sheet, and an atmospheric CO_2 concentration ~~that is~~ three times ~~(3x) of~~ the PI level (Burls et al., 2021). The solar constant, orbital parameters, and aerosol concentration in MCO~~I 3x~~ are kept identical to those of the PI simulation.

To examine the climate response to orbital forcing, we conducted sensitivity simulations by modifying orbital parameters in each baseline experiment. For both the PI and MCO climate, we performed a ~~A~~ "winter~~cold~~ perihelion~~orbit~~" simulation with minimum boreal~~NH~~ summer insolation (~~orb~~NSI_min), and a "summer~~warm~~ perihelion~~orbit~~" simulation with maximum ~~NH~~ boreal summer insolation (~~orb~~NSI_max) ~~were performed for both the PI and the Miocene~~ (Table S1). These orbital simulations are designed to represent mid- to late Miocene intervals characterized by pronounced $\delta^{13}C$ excursions and widespread carbon burial associated with the Monterey events (Anttila et al., 2023; Holbourn et al., 2018; Westerhold et al., 2020)~~Our Miocene simulation focus on the mid-to-late Miocene (11–10 Ma), a period marked by pronounced $\delta^{13}C$ excursion and widespread carbon burial associated with the Monterey carbon isotope events (Anttila et al., 2023; Holbourn et al., 2018; Westerhold et al., 2020)~~. Specifically, we selected two representative time slices at 10.777 Ma (NSI_max~~insolation maximum~~) and 10.767 Ma (NSI_min~~insolation minimum~~) ~~as representative time slices~~ (Fig. S1). This orbital sensitivity framework~~approaches~~ has~~ve~~ been widely ~~used~~ applied in previous Pleistocene studies (Battisti et al., 2014; Bosmans et al., 2018; Dai et al., 2024). Although eccentricity also differs between these configurations, eccentricity effects are not isolate here and will be addressed in future work targeting the ~400-kyr cycle.

Table 1. Model simulation setup

Simulation	Geography Setting	pCO_2 (ppm)	Orbital forcing			Duration of simulation (yrs)	TOA* (W/m^2)	GMAT** (°C)
			Eccentr	Obliquity (rad)	Long. Perih			
PI	Modern	280	0.0167	0.4091	102.040°	1700	-0.04	15.61
PI_NSImax			0.0508	0.4208	281.387°	300	0.05	15.75
PI_NSImin			0.0599	0.3983	68.158°	300	-0.17	15.71
MCO	Miocene (~15Ma)	840	0.0167	0.4091	102.040°	1700	0.34	22.32
MCO_NSImax			0.0508	0.4208	281.387°	400	0.28	22.47
MCO_NSImin			0.0599	0.3983	68.158°	400	0.30	22.58
MCO_1x		280	0.0167	0.4091	102.040°	1000	0.15	22.58

TOA*: Top-of-Atmosphere (TOA) radiation imbalance; GMAT**: Global Mean Air Temperature

The ~~NH~~ June insolation contrast between NIS~~these two~~ max and NISmin ~~cases~~is substantial: reaches 130 W/m^2 at 65 °N and 90 W/m^2 at 20 °N (Fig. S1 & S2). Th~~i~~se seasonal insolation anomalies~~difference~~ primarily results from ~~the change~~differences in the longitude of perihelion (~~:~~281 °and 68 °), corresponding ~~roughly~~ to boreal summer and winter occurring near~~at~~ perihelion, respectively (Fig. S1 & Table S1). In ~~orb~~NISmax, ~~Earth receives more~~enhanced ~~insolation during~~ boreal summer insolation and reduced ~~less during~~ winter insolation ~~,~~ amplify~~ing~~ the globally averaged~~a~~ annual insolation cycle by ~80 W/m^2 relative to the baseline, whereas~~. Conversely,~~ NSI~~orb~~min

weakens~~reduces~~ the annual cycle by 60 W/m^2 (Fig. 1d). Meridionally, ~~orbmax~~ NSImax increases annual-mean insolation at high-latitudes while slightly reducing it in the tropics due to its higher obliquity, with the opposite pattern ~~observed~~ in NSI~~orb~~min (Fig. 1c).

~~Notably, although these configurations are specific to the Miocene, similar orbital patterns also recur throughout the Pleistocene (Fig. S3).~~ Applying these orbital forcings ~~to the PI and Miocene baseline simulations~~ yields two pairs of experiments: PI~~orb~~_NSImax/PI_NSI~~orb~~min for the pre-industrial ~~period~~ and MCO_NSI~~Iorbm~~max/MCO_NSI~~MIorb~~min for the Miocene. It worth to note that although these specific configurations are chosen for the Miocene, similar orbital patterns recur throughout the Pleistocene (Fig. S3).

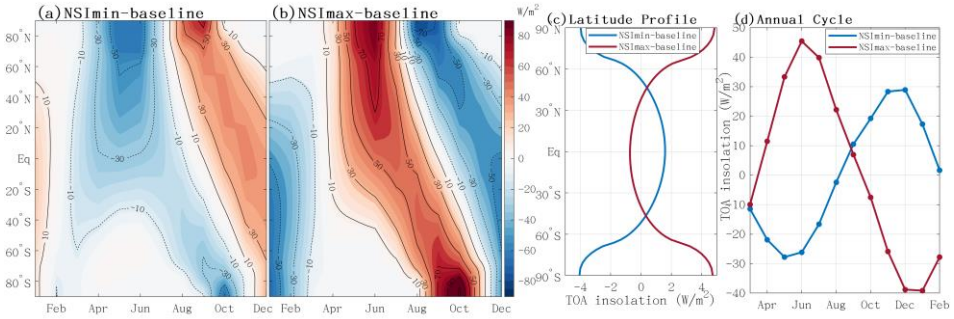

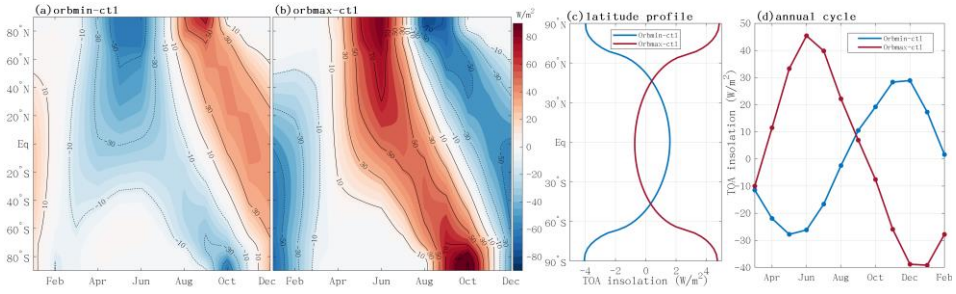

Figure 1. Orbital-induced insolation changes (W/m^2) of the NSI~~orb~~min (a) and NSI~~orb~~max (b) simulations from the baseline simulation, and their latitude profile of annual-mean insolation (c) and globally averaged annual insolation cycle (d).

Both~~The~~ PI and MCO~~I 3X~~ baseline simulations were each run for 1700 years to reach quasi-equilibrium. ~~The o~~Orbital simulations were then branched from the year 1601th of the corresponding~~PI and Miocene~~ baseline runs and integrated for additional 300 (PI_NSImax, PI_NSImin) and 400 years (MCO_NSImax, MCO_NSImin), respectively. Over the final 100 years of each experiments, ~~This approach ensured that~~ the global mean t~~T~~op-of-Atmosphere (TOA) radiation imbalance within ±0.34 W/m^2 (Table. S1) ~~over the final 100 years~~. Monthly means

~~output~~ from these equilibrated periods~~simulations~~ are~~were~~ used for all subsequent analysis. The PI simulation reasonably captures the spatial pattern and magnitude of present-day seasonal temperature variations ~~in both magnitude and spatial pattern~~ relative to~~, closely matching~~ the CMIP5 multi-model mean and ERA5, with ~~data despite~~ a minor cold bias in Arctic Eurasia linked to excessive ~~due to~~ sea ice ~~overestimation~~ (see SI for more details).

2.2 Diagnostic analysis

To diagnose the processes controlling the temperature response to orbital forcing, ~~W~~we ~~conducted~~ apply a one-dimensional Energy Balance Model ananlysis (EBM) following ~~(~~Heinemann et al.~~,~~ (2009) and ~~;~~ Wei et al.~~,~~ (2023). ~~to quantify how changes in radiative components contribute to temperature response to orbital forcing.~~ The EBM balances net incoming shortwave radiation against~~with~~ outgoing longwave radiation and meridional heat transport, using radiative fluxes from the coupled general circulation model (GCM) as input. Temperature differences between simulations are decomposed into contributions from ~~change in~~ surface albedo, water-vapor greenhouse trapping~~gas of water vapor~~, cloud radiative effects, ~~surface albedo,~~ and meridional heat transport~~, and cloud~~. C~~The c~~loud effects ~~can be~~are further decomposed into shortwave and longwave components.

The EBM components reproduce the zonal-mean temperature responses simulated by ~~align well with~~ the GCM~~, simulated results, effectively capturing the zonal-mean features of temperature response,~~ with deviations generally within~~of~~ 0.1-0.9 ℃ (Fig. S4). Slight underestimat~~es~~ions occur in the NH subtropics and~~,~~ polar regions~~, and high-latitude Southern Ocean~~, while ~~an~~ overestimation appears near~~around~~ 70-80 ℃N ~~latitudinal~~ (Fig. S4)~~. These slight discrepancies are~~ consistent with~~similar in magnitude to those reported in the~~ previous studies and mainly reflecting nonlinear processes associated with ~~arise from~~ seasonal and zonal averaging ~~of nonlinear processes~~ (Lunt et al., 2012). The EBM decomposition is used to interpret the relative roles of albedo, water vapour, clouds, and heat transport in shaping the spatial structure of orbital-scale temperature changes.

3 Results and Discussion

3.1 Weaker seasonality of temperature response during the Miocene

The annual temperature cycle in the MCO is 3.2 ℃, smaller than the 3.7℃ in PI, reflecting reduced July warming and weaker January cooling (Fig 2a). The MCO-1x simulation show an intermediate amplitude of ~3.5 ℃ (Fig. S4), suggesting both elevated CO_2 and Miocene boundary condition contribute to the reduced seasonality, with the latter exerting a slightly larger influence.

Orbital forcing substantially modulates the amplitude of the seasonal temperature cycle~~variations~~. Reduced boreal summer insolation weakens the seasonal cycle ~~, from 3.2 ℃ in MI-3x~~ by 1.9 to 1.3 ℃ in MCO_NSI~~MIorb~~min, and by 2. ~~from 3.7℃ in PI~~ to 1.6 ℃ in ~~PIorbmin~~PI_NSImin. Conversely, increased boreal summer insolation intensifies seasonality, raising~~reach~~ing it to 5.4 ℃ in MCO~~I~~NSI~~orb~~max and 6.4 ℃ in PINSI~~orb~~max (Fig. 2). Consequently, seasona~~l~~ l global-mean air temperature (GMAT) variations rise by more than 2 ℃ in the NSI~~orb~~max simulations and

decline by a similar magnitude in the NSI~~orb~~min simulations relative to their respective baselines. The~~se changes in~~ JJA temperature differences between NSImax and NSImin exceed 2.5 ℃ ~~between orbital simulations~~ (Fig. 2)~~, a shift~~ comparable to the ~3 ℃ global cooling during the late Miocene (Westerhold et al., 2020), underscoring the potential ~~role~~ of orbital forcing to generate large-amplitude~~in~~ climate variability.

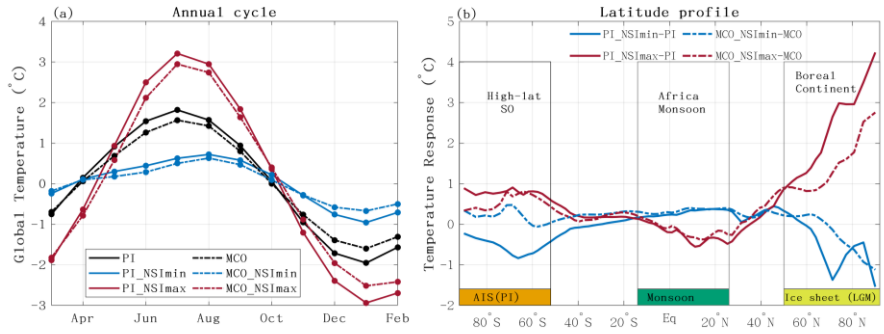

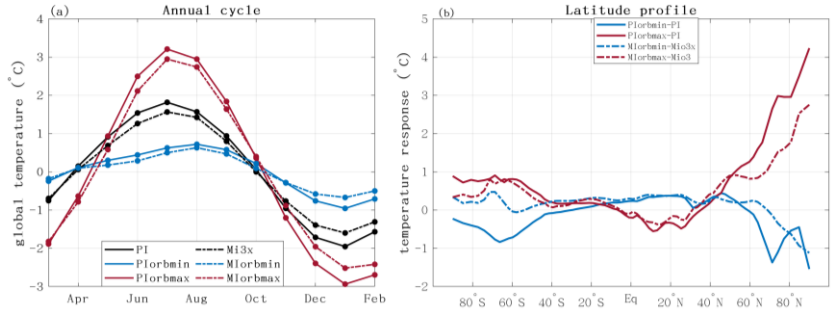

Figure 2. (a) Annual cycle of temperature anomalies relative to ~~(from~~ the~~ir~~ annual mean) ~~(a)~~, with black, red and blue lines representing baseline, NSI_max and NSI_min simulations, respectively. Solid lines denote the PI climate, and dashed lines denote the Miocene climate. (b) Latitude profile of temperature response to orbital forcing, shown as anomalies to their baseline simulation and using the same color scheme as in (a). The locations of modern Antarctic Ice sheet (AIS), major monsoon regions and the Last glacial maximum Ice sheets are indicated in (b).

~~and their latitude profile of temperature response to orbital forcing (b).~~

Compared with~~to~~ the PI climate~~context~~, the MCO~~I 3x~~ simulation exhibits weaker seasonality and a dampened orbital response (Fig. 2a). ~~The annual cycle is smaller in MI 3x than in PI, reflecting reduced July warming and January cooling.~~ The GMAT response to orbital forcing is diminished by ~~approximately~~ ~ 0.1 ℃ in both MCO~~i~~_~~orb~~NSImin and MCO_~~Iorb~~NSImax simulations, yield~~lead~~ing ~~to~~ ~10 % weaker changes in seasonal amplitude ~~changes~~. This diminished Miocene temperature response is also evident in the latitudinal profile, showing differences of up to 1 ℃ at high latitudes (Fig. 2b). Because comparable analyses are not yet available for other

warm climate intervals, it remains uncertain whether the reduced orbital response identified here is specific to the MCO or reflect a more general feature of warm climate states. This question requires further investigation.

This reduced Miocene seasonality is consistent with proxy-based evidence for weaker~~indicating lower~~ seasonality during the warming Miocene in Europe (Harzhauser et al., 2011), the Mediterranean (Utescher et al., 2009), and N America (Reichgelt et al., 2023). Variation in Miocene~~'s~~ seasonal response to identical orbital forcing can alter the relationship between growing-season and annual mean temperatures, potentially biasing proxy-based climate reconstructions. This highlight the importance of applying seasonality adjustments that account for different paleoclimate background~~contexts~~, rather than relying solely on modern analogues, when addressing well-documented seasonal biases in proxies (Bova et al., 2021; Marsicek et al., 2018; Laepple and Lohmann, 2009; Laepple et al., 2022).

3.2 Spatially varied Miocene temperature responses

The NIS~~orb~~max and NSI~~orb~~min simulations show overall anti-phased annual mean temperature responses (Fig. 3). Compared to the MCO~~I 3x~~ and PI baselines, NSI~~orb~~max simulations show a dipole pattern, with polar warming but cooling in the tropics and subtropics of both hemispheres. Conversely, NSI~~orb~~min simulations show high-latidue ~~an opposing dipole:~~ cooling ~~at high latitudes~~ and extratropical and tropical warming ~~in the tropics~~that~~,~~ extending up to ~60 ºN and 40 ºS. Similar high versus ~~-~~low~~-~~ latitude contrasts have been reported in simulations of interglacials characterized by high obliquity and precession, such as Mid-Holocene (Brierley et al., 2020; Dai et al., 2024) and other interglacials [Yin and Berger, 2012; Herold et al 2012]. These patterns are primar~~i~~ily related to the change in obliquity and precession, and are further amplified by feedback including high-latitude albedo changes and shifts in the tropical hydrological cycle (Fig. S5 & S6).

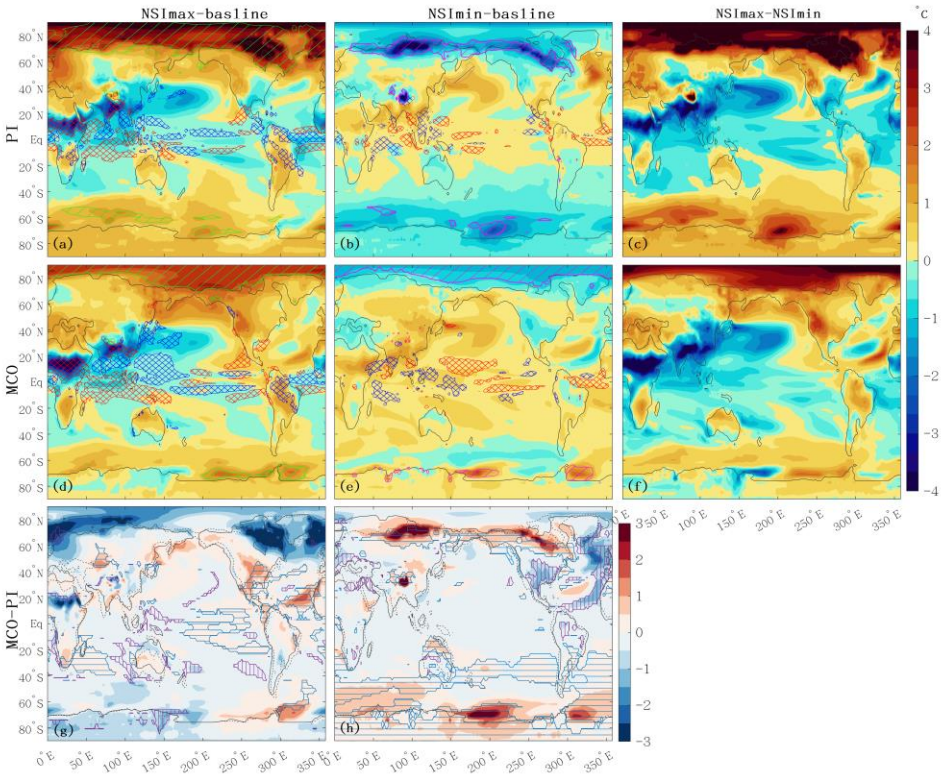
NSImax-basline
NSImin-basline
NSImax-NSImin
°c
PI
MCO
MCO-PI
(a)
(b)
(c)
(d)
(e)
(f)
(g)
(h)

253

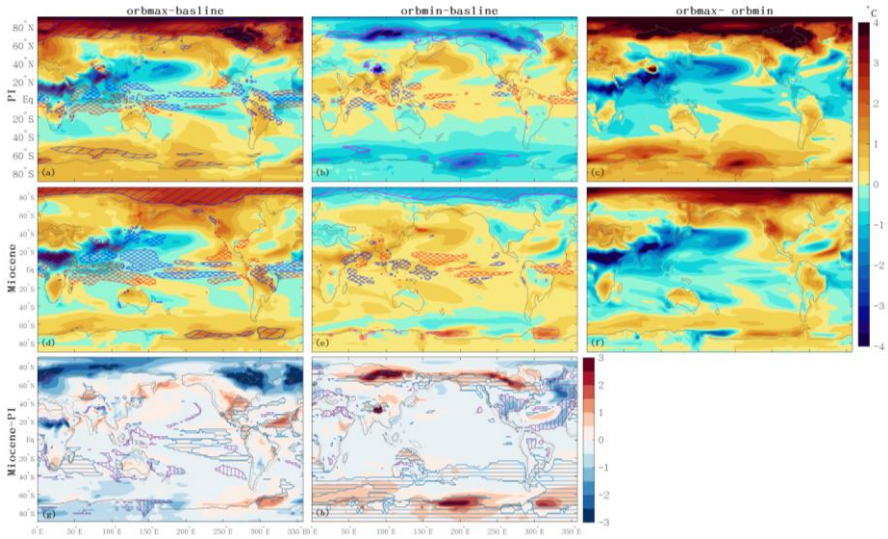

Figure 3. Annual- mean air temperature response (℃). Upper panel: Anomalies of NSImax and NSImin simulations relative to the baseline simulation (a, b) and the difference between NSImax and NSImin simulations (c), all for the PI. Cross marked regions indicate where precipitation increased (red) or decreased (blue) by more than 0.6 mm/day. Hatching indicates regions where albedo increase (magenta) or decrease (green) by over 5%. Middle panel:Same as upper panel but for the Miocene. Lower panel: Differences between the Miocene and PI baseline simulations for the NSImax (g) and for the NSImin (h).Blue horizontal and purple vertical hatching regions indicate where the sign of anomalies is reversed—shifting from negative in PI to positive in Miocene, and vice versa ~~to orbital forcing, with anomalies relative to baseline simulations displayed in the top two panels. Crosses mark areas where precipitation increased (red) or decreased (blue) by more than 0.6 mm/day. Hatching indicates regions where albedo increase (magenta) or decrease (blue) by over 5%. The last column summarized orbmax-orbmin differences. The bottom panel highlights differences between PI and Miocene response; blue horizontal and purple vertical hatching marking regions where the sign of anomalies is reversed — shifting from negative in PI to positive in Miocene, and vice versa~~.

3.2.1 Reduced High-latitude Orbital Response in the Miocene

Compared to PI, the Miocene orbital response is notably weaker at high northern latitudes (Fig. 3). Under ~~the~~ PI condition~~text~~, the strongest ~~warming in~~ PINSI~~orb~~max warming (~4.8 ℃) occurs over northeast Canada and the Labrador Sea, whereas the MCO_NSI~~Iorb~~max warming is less than half as large~~strong~~ (Fig. 3b). Similarly, cooling in the PINSI~~orb~~min simulation reaches `4.4 ℃ over Western Siberia, but only `1 ℃ in MCO_~~Iorb~~NSImin (Fig. 3a, 3c). The strongest Miocene ~~orbital~~ response —2.8℃ over the Chukchi Sea—remain~~i~~s ~~still~~ weaker than its~~in~~ PI counterpart.

~~The~~ EBA results show that much of the weaker Miocene temperature responses in NH high-latitudes can be attributed to smaller changes in surface albedo (Fig. 4). In the Miocene, the albedo contribution is roughly half of that in the PI. For example, albedo-driven warming reaches 6 ℃ in PINSI~~orb~~max but only ~3 ℃ in MINSI~~orb~~max. Similarly, MCONSI~~Iorb~~min shows poleward-shifted and weaker albedo-driven cooling than PINSI~~orb~~min. This

reduced albedo feedback dampens the Miocene temperature responses to orbital forcing, with temperature changes closely matching the spatial pattern of albedo response ~~variations~~ (Fig. 3). Further analysis (Fig. S6) shows ~~reveals~~ that strong albedo changes in~~under~~ the PI simulation~~contexts~~ coincides with ice sheets and sea ice, where ice–albedo feedbacks amplify~~enhance~~ the climate~~'s~~ response to orbital forcing. By contrast, the warmer Miocene climate, characterized by widespread vegetation, limited sea ice, and lower surface albedo, is less sensitive to orbital perturbations~~forcing~~.

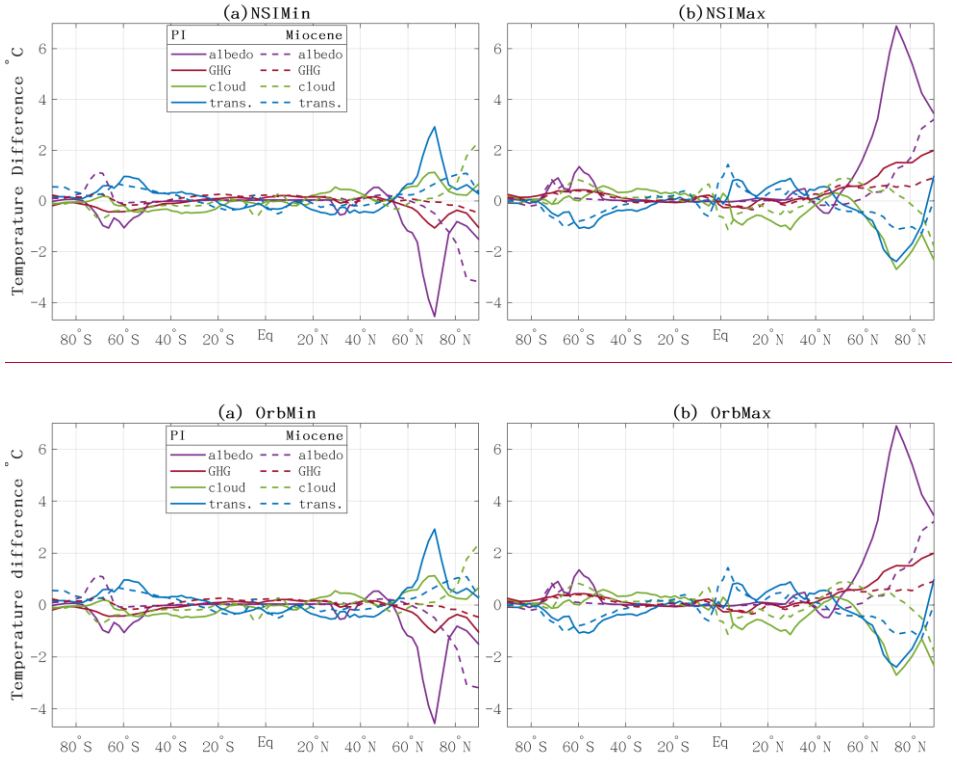

Figure 4. Zonal mean surface temperature responses ~~(~~to orbital forcing from~~insolation) of~~ the EBM decomposition. ~~various components from energy balance analysis.~~ Total response is decomposed into contributions from the surface albedo (albedo), water vapor's greenhouse (GHG), meridional heat transport (trans), and cloud effects (cloud).

The ~~above~~ strong albedo response is further reinforced by water-vapor~~'s~~ greenhouse effect but partly offset ~~is counteracted~~ by cloud changes~~over~~. Water-vapor contributions largely follow albedo patterns, reflecting their dependence on surface energy availability, whereas clouds exert an opposing influence. Further decomposition into shortwave and longwave components reveal that shortwave cloud radiative~~on~~ effects dominates, yield~~indicat~~ing a generally weaker net negative feedback in the Miocene (Fig. S4).

These results are consistent with previous studies suggesting weaker climate sensitivity during warm periods [*De Vleeschouwer et al., 2017; Levy et al., 2019; Naish et al., 2009*](Reichgelt et al., 2023; *De Vleeschouwer et al.*, 2017; *Levy et al.*, 2019; *Naish et al.*, 2009). For example, proxy reconstruction indicates muted Miocene climate variability in eastern North America compared to the modern era (Reichgelt et al., 2023). The larger and more regular temperature variations in the PI simulation point tosuggest an enhanced sensitivity to orbital forcing, consistent with the development of pronounced NH glacial-interglacial cycles. In contrast, the Miocene's dampened response implies weakened climate response to orbital forcing and thus possibly reduced amplitude of that climate variability was likely less periodic or characterized by a more prolonged cycle under warmer backgroundclimate conditions.

3.2.2 Enhanced tropical North Africa cooling in the MCOINSIorbmax simulation

An exception to the weaker Miocene response is the enhanced tropical North Africa cooling in the MCO_NSIMIorbmax simulation (Fig. 3d). Here, annual-mean temperature decrease bywhich shows a 4.4 °C decrease—greater than the 3.8 °C in PI_orbNSImax—and the anomaly extends farther north. Seasonal decomposition indicates that this cooling persists even during boreal summer, despite increased insolation (Fig. S1 & S7). It coincides with intensified precipitation, indicatingpointing to a dominant role of insolation-driven hydrological changes in controlmodulating temperature.

These enhanced Miocene cooling effects under MCO_NSImax are consistent with increased precipitation. The EBM results show that the stronger cooling in the MSIorbmax simulation arises from larger water-vapor and cloud contributionhanges (-0.34 and -1.12°C in Miocene vs. 0.28 and 0.94°C in PI). These enhanced Miocene cooling effects align with increased precipitation. Additional analysis of mositurewater flux divergence suggests that more moisture is from the Tethys Sea during the Miocene, feedings this region's precipitation over tropical North Africa (Fig. S8). This highlights that a A wider Tethys Sea provides an efficient moisture source, while a warmer climate accelerates the hydrological cycle (Fig. S8) (Sarr et al., 2022; Huntington, 2006). These findings are in linealign with proxy evidence for intensified hydrological cycle and increased precipitation under warm climate, such as the "green Sahara" during the mid-Holocene (Hoelzmann et al., 2001; Kutzbach and Liu, 1997; Liu et al., 2024), and supporting the interpretationconclusion that MCONSIorbmax cooling is driven by hydrological intensification. Similar deep-time sensitivity to orbital forcing has been noted in early Cenozoic simulationprevious studies, which show found substantial precipitation responses comparable to monsoon signalsduring the early Cenozoic, comparable to monsoon signals (Zhang et al., 2024).

3.2.3 Disrupted Southern Ocean warming orbital signal in the MCO_NSIminMiocene

In the Southern Ocean, the Miocene response to orbital forcing deviates from the expected anti-phase pattern observed in PI that roughly follows insolation change. In MCO_NSImin simulation,Specifically, unexpected warming occurs over the Ross Sea and Weddell Sea despite reduced local annual-mean insolation,in response to overall reduced local annual mean insolation in the MIorbmin simulation, in contrasted to with the cooling

simulated~~observed~~ in PINSI~~orb~~min. This Miocene response deviates from the the near-symmetric responses observed in PI, which broadly follows local insolation changes.

This anomalous warming is particularly evident during~~in the~~ austral winter (Fig. S10), disrupting the expected anti-phase signal and generating an out-of-phase response~~pattern~~. ~~According to~~ EBM analysis indicates that~~,~~ the reversed temperature response in MCONSI~~I~~~~orb~~min (1.1℃ warming at 71 ℃S instead of cooling) is mainly attributed to albedo and water~~-~~ vapor effects (Fig. 4). During the Miocene, the maximum sea~~-~~ice edge lies closer to the pole (~~extended polarward around~~ 70°S), where significant winter insolation anomalies~~changes~~ (Fig. S9) promote~~facilitated increased austral winter insolation to trigger~~ positive ice-albedo feedback:~~—~~, reducing sea ice and enhanced ocean-atmosphere heat exchange,~~warming (Fig. 3 & S10)—~~ and additional~~generating more~~ atmospheric water vapor (Fig. 3 & S10). In contrast, PI sea ice extend~~sed in~~to lower latitudes, where insolation changes were smaller, limit~~reduc~~ing sensitivity to~~ the~~ seasonal ~~change of~~ orbital forcing (Fig. S10).

These results support geological evidence that ocean-atmosphere-ice sheet interactions amplified Antarctic ice-sheets sensitivity to orbital forcing during~~ their~~ Miocene ice-sheet growth~~expansion~~ [*De Vleeschouwer et al.*, 2017; *Levy et al.*, 2019; *Naish et al.*, 2009]. Sediment records further indicate a stronger and more stable climate response as~~with growth of~~ ice sheets and sea ice expanded,~~(De Vleeschouwer et al., 2017; Levy et al., 2019; Naish et al., 2009; Reichgelt et al., 2023),~~ compared with~~to~~ warmer periods~~,~~ such as~~like~~ the Early Eocene~~,~~, when ~~intensified~~ carbon-climate coupling ~~played a dominant role~~dominated (De Vleeschouwer et al., 2017; Levy et al., 2019; Naish et al., 2009; Reichgelt et al., 2023)~~,~~(Setty et al., 2023). Overall, these findings underscore strong background-state control on ~~how~~ Southern Ocean sea~~-~~ice feedbacks ~~are strongly modulated by the background climate state~~ (Bloch‐Johnson et al., 2021).

域代码已更改

3.3 Spatially divere~~Irregulate~~ Miocene responses to orbital forcing and ~~reduced~~ weakened internal climate variability

Beyond differences in magnitude, the spatial extent of warming and cooling response also differs ~~notably~~ between the PI and Miocene simulation. Under~~In the~~ PI conditions, high-latitude temperature responses are large~~strict~~ly sysmetric~~anti-phased~~ between NSImax and NSImin~~two insolation cases~~. In contrast, the Miocene simulations show warming in both MCONSI~~orb~~min and MCO_~~orb~~NSImax over Siberia and Alaska, resulting in distinct regional responses across 60-70 ℃N~~,~~ spanning Eurasia, Alaska and North America continent (Fig. 3e, blue line). Similarly, the Weddell Sea and Ross Sea exhibit~~in the Southern Ocean show~~ overall warming in both Miocene orbital simulations, deviating from the ~~expected anti-phased~~symatric PI behavior~~changes observed in the PI~~ (Fig. 3 & S11). These deviations suggest a less systematic and less predictable Miocene ~~climate~~ response~~system,~~, likely consistent with proxy evidence for ~~reflecting the~~ dominance of longer-period orbital variability ~~periodicities~~ (~~, such as~~e.g. the 400-kyr~~a) cycle,~~ rather than ~~the~~ 40 kyr~~a~~ and 100 kyr~~a~~ cycle characteristic of the Pleistocene~~, as suggested by proxy records~~ [Holbourn et al., 2007; Tian et al., 2013; Westerhold et al., 2020; Liu et al., 2024]. This also implies that simpl~~ey comparing~~ NSI~~orb~~max minus NSI~~orb~~min, without examining spatial patterns in detail, can~~risks missing~~obscure nonlinear responses—particularly under warmer background conditions~~limate conditions~~.

In addition to meanseasonal changes, internal temperature variability is crucial for assessingprovides insight into climate stability (Harzhauser et al., 2011). We thereforeTo investigate this, we examine deseasonalised variability (expressed as the (standard deviation) across aboveover key high-latitude regions where major of active glacial dynamics occur. Results show that mMid-latitude Eurasia and North America exhibit higher internal temperature variability in the PI simulation, which is further amplified inunder both PINSIorbmin and PINSIorbmax, reflecting such aenhanceds ice-albedo interactions and land-atmosphere coupling. By contrast, the Miocene showed lower variability is lower and in those regions, further reduced in the MCONSIIorbmin simulation (Fig. 5), suggesting a more stable high-latitude climate with dampened feedbacks under warmer background conditions. Reduced eEastern Pacific variability in the Miocene likely reflects enhanced inter-basin exchange through an open Panama Seaway, which buffers regional responses. The Sstronger and more regular PItemperature variability in the PI simulations indicatessupports greater orbital sensitivity and support the development of pronounced NH glacial-interglacial cycles, whereas, whereas the dampened and irregular Miocene response suggests weaker or less periodic orbital pacingcycles under warm conditions.

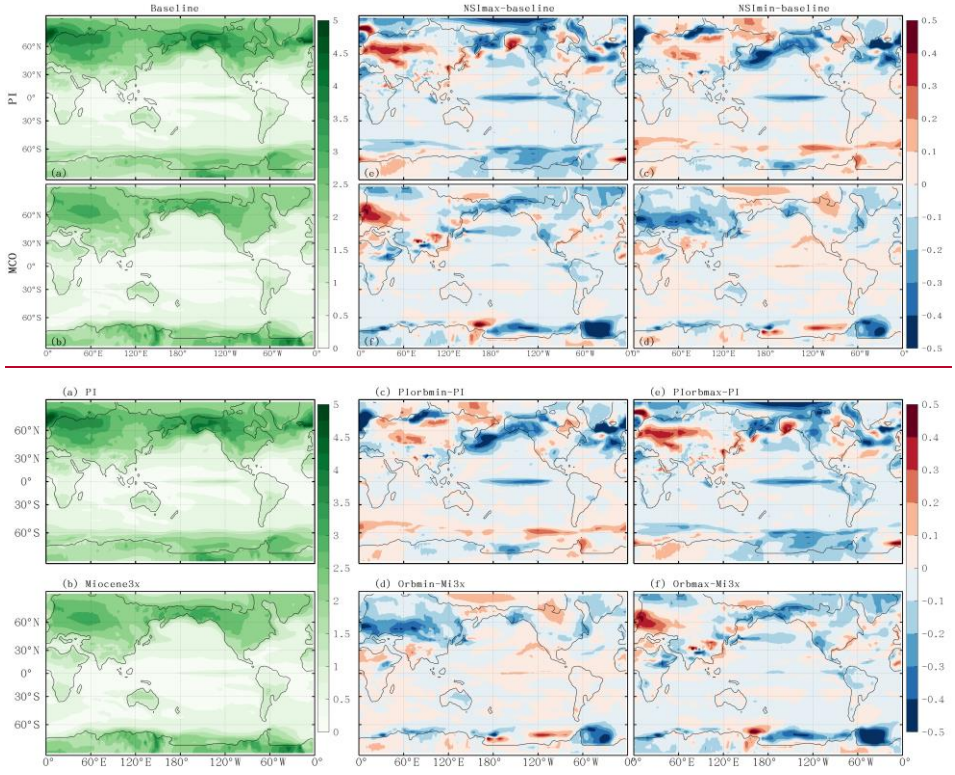

Figure 5. Standard deviation of deseasonalized temperature, and their its responses to orbital forcing.

4 Conclusions and Implications

The Miocene, particularly the interval following the Miocene Climatic Optimum (MCO), shows strong orbital pacing in geological records despite warm boundary conditions, limited Northern Hemisphere ice, and reduced meridional temperature gradients. However, the mechanisms linking orbital forcing to climate variability during this warm epoch are not well understood. By conducting parallel orbital sensitivity experiments under mid-Miocene and pre-industrial (PI) conditions, we evaluate how background climate state modulates the expression of orbital-driven temperature change. ~~Orbital insolation drives glacial-interglacial cycles through complex feedbacks involving continental ice sheets. While most studies have focused on the Quaternary—when large continental ice sheets presented in both hemispheres—the climate response to orbital forcing during warm periods, such as during the Miocene, remains less well understood. This study addresses that gap by conducting and comparing two sets of orbital sensitivity simulations under pre-industrial (PI) and mid-Miocene conditions, each forced with minimum (orbmin) and maximum (orbmax) boreal summer insolation.~~

In general, ~~The simulations reveal~~both climates exhibit~~an~~ broadly ~~overall~~ anti-phased temperature responses between maximum and minimum boreal summer insolation, each characterized by a meridional high-to-low latitude dipole,~~between, the two orbital scenarios: Orbmax leads to high-latitude warming and tropical cooling,~~ However,~~whereas~~ the Miocene response is ~1°C weaker, with~~orbmin produces the opposite pattern. However, compared to PI, the Miocene exhibits a weaker global temperature response (~1°C smaller)~~ regionally dependent contrasts and~~ and~~ reduced symmetric between two orbital cases~~less stable anti-phased behavior among orbmax and orbmin~~. Three ~~K~~key differences emerge~~include~~: (1) ~~Weaker~~ Reduced ~~temperature response over~~ Northern Hemisphere continental sensitivity~~s~~ in the Miocene, ~~caused by reduced~~reflecting weaker surface~~-~~albedo, ~~feedbacks primarily due to different vegetation and ice cover, along with contributions from~~ water~~-~~vapor, and ~~greenhouse effect and~~ cloud radiative effects in a warmer, low-ice, vegetation-modified climate—consistent with proxy evidence for diminished high-latitude climate sensitivity after the MCO~~cover~~; (2) Stronger hydrological~~co~~ cooling ~~(4.4°C) over~~ in North Tropical Africa in ~~the~~ MCONSI~~orb~~max ~~simulation~~, ~~compared to 3.8°C in PI~~orbmax driven by enhanced ~~,~~precipitation, cloud, and moisture-feedbacks within an intensified~~driven by enhance~~ Miocene~~d~~ hydrological cycle supported by ~~changes due to more moisture from~~ a wider Tethys Sea ~~u—nder the warmer background climate~~indicating amplified hydrological sensitivity to orbital forcing in warm climates; and (3) a ~~Out-of-phase~~reversed ~~temperature response in the~~ Southern Ocean warming in ~~the~~ MCONSI~~orb~~min under lower insolation, where poleward-restricted Miocene sea ice allows ~~simulation, driven by increased austral~~ winter insolation anomalies to trigger positive ice-albedo feedbacks, ~~sea ice reduction, and subsequent positive ice-albedo feedbacks~~matching proxy evidence for heightened Antarctic obliquity sensitivity.

These differences highlight that the strength and structure of orbital responses depend strongly on background climate state. The Miocene's weaker seasonal amplitude and reduced internal variability imply diminished and less periodic orbital pacing relative to the PI climate, consistent with dominant 400-kyr eccentricity variability in Miocene proxy records. This has two key implications~~distinct responses have two major climate implications~~: First, Miocene proxy reconstructions may overestimate annual mean temperatures if modern seasonal analogues are

applied, underscoring the need for context-specific seasonality corrections; and~~the weaker Miocene seasonal response alters the difference between growing-season and annual-mean temperatures. This mismatch may lead to overestimates of annual-mean temperature reconstruction based on some proxy records, highlighting the need for context-specific seasonality corrections rather than reliance on modern analogs (Bova et al., 2021; Marsicek et al., 2018; Laepple and Lohmann, 2009; Laepple et al., 2022).~~ Second, the stronger and more sysmatic PI response reflects the emergence of high-latitude cryosphere feedbacks central to Quaternary glacial–interglacial cycles.~~, the larger and more regular temperature variability in the PI context indicates stronger sensitivity to orbital forcing and supports the presence of well-developed NH glacial–interglacial cycles. In contrast, the Miocene's subdued and irregular climate variability suggests weaker and less periodic orbital pacing under warmer conditions, consistent with proxy evidence [*Holbourn et al.*, 2013; *Holbourn et al.*, 2018; *Steinthorsdottir et al.*, 2021; *Westerhold et al.*, 2020].~~

Acknowledgments

The authors are grateful to the two anonymous referees for their valuable comments that substantially improved the manuscript, as well as the Editor, Ran Feng, for managingthe review process. This study was supported by the National Key R&D program of China (2023YFF0803902) and (2023YFF0803904). We appreciate the technical support of the National Large Scientific and Technological Infrastructure, *Earth System Numerical Simulation Facility* (https://cstr.cn/31134.02.EL).

Open Research

Model output data from this study are available at Zhang (2025).

Author contributions

Conceptualization & Study Design: YZ;

Methodology & Simulations: YZ, JW, with support from WZ;

Formal Analysis & Investigation: YZ, with guidance from YQ, A. de B., ZS, LZ;

Data Curation: ZL, ND;

Writing – Original Draft: YZ;

Writing – Review & Editing: All authors.

Competing interests

Some authors are members of the editorial board of journal Climate of the Past.

References

Anttila, E. S. C., Macdonald, F. A., Szymanowski, D., Schoene, B., Kylander-Clark, A., Danhof, C., and Jones, D. S.: Timing and tempo of organic carbon burial in the Monterey Formation of the Santa Barbara Basin and relationships with Miocene climate, Earth and Planetary Science Letters, 620, 10.1016/j.epsl.2023.118343, 2023.

Battisti, D. S., Ding, Q., and Roe, G. H.: Coherent pan-Asian climatic and isotopic response to orbital forcing of tropical insolation, Journal of Geophysical Research: Atmospheres, 119, 10.1002/2014jd021960, 2014.

Berger: Long-Term Variations of Daily Insolation and Quaternary Climatic Changes %J Journal of Atmospheric Sciences, 35, 2362-2367, https://doi.org/10.1175/1520-0469(1978)035<2362:LTVODI>2.0.CO;2, 1978.

Berger, Yin, Q., and Wu, Z.: Length of astronomical seasons, total and average insolation over seasons, Quaternary Science Reviews, 334, 108620, https://doi.org/10.1016/j.quascirev.2024.108620, 2024.

Bloch-Johnson, J., Rugenstein, M., Stolpe, M. B., Rohrschneider, T., Zheng, Y., and Gregory, J. M.: Climate Sensitivity Increases Under Higher CO2 Levels Due to Feedback Temperature Dependence, Geophysical Research Letters, 48, 10.1029/2020gl089074, 2021.

Bosmans, J. H. C., Erb, M. P., Dolan, A. M., Drijfhout, S. S., Tuenter, E., Hilgen, F. J., Edge, D., Pope, J. O., and Lourens, L. J.: Response of the Asian summer monsoons to idealized precession and obliquity forcing in a set of GCMs, Quaternary Science Reviews, 188, 121-135, 10.1016/j.quascirev.2018.03.025, 2018.

Bova, S., Rosenthal, Y., Liu, Z., Godad, S. P., and Yan, M.: Seasonal origin of the thermal maxima at the Holocene and the last interglacial, Nature, 589, 548-553, 10.1038/s41586-020-03155-x, 2021.

Brierley, C. M., Zhao, A., Harrison, S. P., Braconnot, P., Williams, C. J. R., Thornalley, D. J. R., Shi, X., Peterschmitt, J.-Y., Ohgaito, R., Kaufman, D. S., Kageyama, M., Hargreaves, J. C., Erb, M. P., Emile-Geay, J., D'Agostino, R., Chandan, D., Carré, M., Bartlein, P. J., Zheng, W., Zhang, Z., Zhang, Q., Yang, H., Volodin, E. M., Tomas, R. A., Routson, C., Peltier, W. R., Otto-Bliesner, B., Morozova, P. A., McKay, N. P., Lohmann, G., Legrande, A. N., Guo, C., Cao, J., Brady, E., Annan, J. D., and Abe-Ouchi, A.: Large-scale features and evaluation of the PMIP4-CMIP6 midHolocene simulations, Climate of the Past, 16, 1847-1872, 10.5194/cp-16-1847-2020, 2020.

Burls, N. J., Bradshaw, C. D., De Boer, A. M., Herold, N., Huber, M., Pound, M., Donnadieu, Y., Farnsworth, A., Frigola, A., Gasson, E., von der Heydt, A. S., Hutchinson, D. K., Knorr, G., Lawrence, K. T., Lear, C. H., Li, X., Lohmann, G., Lunt, D. J., Marzocchi, A., Prange, M., Riihimaki, C. A., Sarr, A. C., Siler, N., and Zhang, Z.: Simulating Miocene Warmth: Insights From an Opportunistic Multi-Model Ensemble (MioMIP1), Paleoceanography and Paleoclimatology, 36, 10.1029/2020pa004054, 2021.

Dai, G., Zhang, Z., Otterå, O. H., Langebroek, P. M., Yan, Q., Zhang, R., and Zhu, Z.: Winter Insolation Modulates Boreal Tropical Monsoonal Temperatures in the Late Pleistocene, Journal of Geophysical Research: Atmospheres, 129, 10.1029/2023jd040577, 2024.

De Vleeschouwer, D., Vahlenkamp, M., Crucifix, M., and Pälike, H.: Alternating Southern and Northern Hemisphere climate response to astronomical forcing during the past 35 m.y, Geology, 45, 375-378, 10.1130/g38663.1, 2017.

Harzhauser, M., Piller, W. E., Müllegger, S., Grunert, P., and Micheels, A.: Changing seasonality patterns in Central Europe from Miocene Climate Optimum to Miocene Climate Transition deduced from the Crassostrea isotope archive, Global and Planetary Change, 76, 77-84, 10.1016/j.gloplacha.2010.12.003, 2011.

Hays, J. D., Imbrie, J., and Shackleton, N. J.: Variations in the Earth's Orbit: Pacemaker of the Ice Ages, 194, 1121-

1132, doi:10.1126/science.194.4270.1121, 1976.

Heinemann, M., Jungclaus, J. H., and Marotzke, J.: Warm Paleocene/Eocene climate as simulated in ECHAM5/MPI-OM, Clim. Past, 5, 785-802, 10.5194/cp-5-785-2009, 2009.

Herold, N., Yin, Q. Z., Karami, M. P., and Berger, A.: Modelling the climatic diversity of the warm interglacials, Quaternary Science Reviews, 56, 126-141, https://doi.org/10.1016/j.quascirev.2012.08.020, 2012.

Hoelzmann, P., Keding, B., Berke, H., Kröpelin, S., and Kruse, H.-J.: Environmental change and archaeology: lake evolution and human occupation in the Eastern Sahara during the Holocene, Palaeogeography, Palaeoclimatology, Palaeoecology, 169, 193-217, https://doi.org/10.1016/S0031-0182(01)00211-5, 2001.

Holbourn, A., Kuhnt, W., Clemens, S., Prell, W., and Andersen, N.: Middle to late Miocene stepwise climate cooling: Evidence from a high-resolution deep water isotope curve spanning 8 million years, Paleoceanography, 28, 688-699, 10.1002/2013pa002538, 2013.

Holbourn, A., Kuhnt, W., Schulz, M., Flores, J.-A., and Andersen, N.: Orbitally-paced climate evolution during the middle Miocene "Monterey" carbon-isotope excursion, Earth and Planetary Science Letters, 261, 534-550, 10.1016/j.epsl.2007.07.026, 2007.

Holbourn, A., Kuhnt, W., Clemens, S. C., Kochhann, K. G. D., Johnck, J., Lubbers, J., and Andersen, N.: Late Miocene climate cooling and intensification of southeast Asian winter monsoon, Nat Commun, 9, 1584, 10.1038/s41467-018-03950-1, 2018.

Huntington, T. G.: Evidence for intensification of the global water cycle: Review and synthesis, Journal of Hydrology, 319, 83-95, https://doi.org/10.1016/j.jhydrol.2005.07.003, 2006.

Kemp, A. E. S., Grigorov, I., Pearce, R. B., and Naveira Garabato, A. C.: Migration of the Antarctic Polar Front through the mid-Pleistocene transition: evidence and climatic implications, Quaternary Science Reviews, 29, 1993-2009, https://doi.org/10.1016/j.quascirev.2010.04.027, 2010.

Kutzbach, J. E. and Liu, Z.: Response of the African monsoon to orbital forcing and ocean feedbacks in the middle holocene, 278, Medium: X; Size: pp. 440-443, 10.1126/science.278.5337.440, 1997.

Laepple and Lohmann, G.: Seasonal cycle as template for climate variability on astronomical timescales, Paleoceanography, 24, 10.1029/2008pa001674, 2009.

Laepple, Shakun, J., He, F., and Marcott, S.: Concerns of assuming linearity in the reconstruction of thermal maxima, Nature, 607, E12-E14, 10.1038/s41586-022-04831-w, 2022.

Laskar, J. A. F. M. G. H. M.: La2010: a new orbital solution for the long-term motion of the Earth, Astronomy & Astrophysics, 532, A89 (2011), 10.1051/0004-6361/201116836, 2010.

Levy, R. H., Meyers, S. R., Naish, T. R., Golledge, N. R., McKay, R. M., Crampton, J. S., DeConto, R. M., De Santis, L., Florindo, F., Gasson, E. G. W., Harwood, D. M., Luyendyk, B. P., Powell, R. D., Clowes, C., and Kulhanek, D. K.: Antarctic ice-sheet sensitivity to obliquity forcing enhanced through ocean connections, Nature Geoscience, 12, 132-137, 10.1038/s41561-018-0284-4, 2019.

Li, L. Y., Yongqiang, Tang, Y., Lin, P., Xie, J., Song, M., Dong, L., Zhou, T., Liu, L., Wang, L., Pu, Y., Chen, X., Chen, L., Xie, Z., Liu, H., Zhang, L., Huang, X., Feng, T., Zheng, W., Xia, K., Liu, H., Liu, J., Wang, Y., Wang, L., Jia, B., Xie, F., Wang, B., Zhao, S., Yu, Z., Zhao, B., and Wei, J.: The Flexible Global Ocean-Atmosphere-Land System Model Grid-Point Version 3 (FGOALS-g3): Description and Evaluation, Journal of Advances in Modeling Earth Systems, 12, 10.1029/2019ms002012, 2020.

Lin, P., Zhao, B., Wei, J., Liu, H., Zhang, W., Chen, X., Jiang, J., Ding, M., Man, W., Jiang, J., Zhang, X., Ding, Y., Bai, W., Jin, C., Yu, Z., Li, Y., Zheng, W., and Zhou, T.: The Super-large Ensemble Experiments of CAS FGOALS-g3, Advances in Atmospheric Sciences, 39, 1746-1765, 10.1007/s00376-022-1439-1, 2022.

Liu, F., Du, J., Huang, E., Ma, W., Ma, X., Lourens, L. J., and Tian, J.: Accelerated marine carbon cycling forced by

tectonic degassing over the Miocene Climate Optimum, Sci Bull (Beijing), 69, 823-832, 10.1016/j.scib.2023.12.052, 2024.

Lunt, D. J., Haywood, A. M., Schmidt, G. A., Salzmann, U., Valdes, P. J., Dowsett, H. J., and Loptson, C. A.: On the causes of mid-Pliocene warmth and polar amplification, Earth and Planetary Science Letters, 321-322, 128-138, 10.1016/j.epsl.2011.12.042, 2012.

Marsicek, J., Shuman, B. N., Bartlein, P. J., Shafer, S. L., and Brewer, S.: Reconciling divergent trends and millennial variations in Holocene temperatures, Nature, 554, 92-96, 10.1038/nature25464, 2018.

Milanković, M. M.: Canon of insolation and the ice-age problem. ~~(Kanon der Erdbestrahlung und seine Anwendung auf das Eiszeitenproblem)~~ Beograd~~lgrade~~, Koninglich Serbische Akademie. 484 pp. [English translation by Israel Porgram for Scientific Translation and published by the U.S. Dept. of Commerce and national Science Foundation.], 1941.~~1941, Kanon der Erdbestrahlung und seine Anwendung auf das Eiszeitenproblem.English, xxiii, 484 p., Israel Program for Scientific Translations; [available from U.S. Dept. of Commerce, Clearinghouse for Federal Scientific and Technical Information, Springfield, Va.], Jerusalem, xxiii, 484 p. pp.1969.~~

Naish, T., Powell, R., Levy, R., Wilson, G., Scherer, R., Talarico, F., Krissek, L., Niessen, F., Pompilio, M., Wilson, T., Carter, L., DeConto, R., Huybers, P., McKay, R., Pollard, D., Ross, J., Winter, D., Barrett, P., Browne, G., Cody, R., Cowan, E., Crampton, J., Dunbar, G., Dunbar, N., Florindo, F., Gebhardt, C., Graham, I., Hannah, M., Hansaraj, D., Harwood, D., Helling, D., Henrys, S., Hinnov, L., Kuhn, G., Kyle, P., Laufer, A., Maffioli, P., Magens, D., Mandernack, K., McIntosh, W., Millan, C., Morin, R., Ohneiser, C., Paulsen, T., Persico, D., Raine, I., Reed, J., Riesselman, C., Sagnotti, L., Schmitt, D., Sjunneskog, C., Strong, P., Taviani, M., Vogel, S., Wilch, T., and Williams, T.: Obliquity-paced Pliocene West Antarctic ice sheet oscillations, Nature, 458, 322-328, 10.1038/nature07867, 2009.

Reichgelt, T., Baumgartner, A., Feng, R., and Willard, D. A.: Poleward amplification, seasonal rainfall and forest heterogeneity in the Miocene of the eastern USA, Global and Planetary Change, 222, 10.1016/j.gloplacha.2023.104073, 2023.

Sarr, A.-C., Donnadieu, Y., Bolton, C. T., Ladant, J.-B., Licht, A., Fluteau, F., Laugié, M., Tardif, D., and Dupont-Nivet, G.: Neogene South Asian monsoon rainfall and wind histories diverged due to topographic effects, Nature Geoscience, 15, 314-319, 10.1038/s41561-022-00919-0, 2022.

Setty, S., Cramwinckel, M. J., van Nes, E. H., van de Leemput, I. A., Dijkstra, H. A., Lourens, L. J., Scheffer, M., and Sluijs, A.: Loss of Earth system resilience during early Eocene transient global warming events, Science Advances, 9, eade5466, 10.1126/sciadv.ade5466, 2023.

Steinthorsdottir, M., Coxall, H. K., de Boer, A. M., Huber, M., Barbolini, N., Bradshaw, C. D., Burls, N. J., Feakins, S. J., Gasson, E., Henderiks, J., Holbourn, A. E., Kiel, S., Kohn, M. J., Knorr, G., Kürschner, W. M., Lear, C. H., Liebrand, D., Lunt, D. J., Mörs, T., Pearson, P. N., Pound, M. J., Stoll, H., and Strömberg, C. A. E.: The Miocene: The Future of the Past, Paleoceanography and Paleoclimatology, 36, 10.1029/2020pa004037, 2021.

Tardif, D., Toumoulin, A., Fluteau, F., Donnadieu, Y., Le Hir, G., Barbolini, N., Licht, A., Ladant, J.-B., Sepulchre, P., Viovy, N., Hoorn, C., and Dupont-Nivet, G.: Orbital variations as a major driver of climate and biome distribution during the greenhouse to icehouse transition, Science Advances, 7, eabh2819, 10.1126/sciadv.abh2819, 2021.

Tian, J., Yang, M., Lyle, M. W., Wilkens, R., and Shackford, J. K.: Obliquity and long eccentricity pacing of the Middle Miocene climate transition, Geochemistry, Geophysics, Geosystems, 14, 1740-1755, 10.1002/ggge.20108, 2013.

Utescher, T., Ivanov, D., Harzhauser, M., Bozukov, V., Ashraf, A. R., Rolf, C., Urbat, M., and Mosbrugger, V.: Cyclic climate and vegetation change in the late Miocene of Western Bulgaria, Palaeogeography, Palaeoclimatology, Palaeoecology, 272, 99-114, 10.1016/j.palaeo.2008.11.014, 2009.

van Peer, T. E., Liebrand, D., Taylor, V. E., Brzelinski, S., Wolf, I., Bornemann, A., Friedrich, O., Bohaty, S. M., Xuan, C., Lippert, P. C., and Wilson, P. A.: Eccentricity pacing and rapid termination of the early Antarctic ice ages, Nat Commun, 15, 10600, 10.1038/s41467-024-54186-1, 2024.

Wang, Y., Yu, Z., Lin, P., Liu, H., Jin, J., Li, L., Tang, Y., Dong, L., Chen, K., Li, Y., Yang, Q., Ding, M., Meng, Y., Zhao, B., Wei, J., Ma, J., and Sun, Z.: FGOALS-g3 Model Datasets for CMIP6 Flux-Anomaly-Forced Model Intercomparison Project, Advances in Atmospheric Sciences, 37, 1093-1101, 10.1007/s00376-020-2045-8, 2020.

Wei, J., Liu, H., Zhao, Y., Lin, P., Yu, Z., Li, L., Xie, J., and Duan, A.: Simulation of the climate and ocean circulations in the Middle Miocene Climate Optimum by a coupled model FGOALS-g3, Palaeogeography, Palaeoclimatology, Palaeoecology, 617, 10.1016/j.palaeo.2023.111509, 2023.

Westerhold, T., Marwan, N., Drury, A. J., Liebrand, D., Agnini, C., Anagnostou, E., Barnet, J. S. K., Bohaty, S. M., De Vleeschouwer, D., Florindo, F., Frederichs, T., Hodell, D. A., Holbourn, A. E., Kroon, D., Lauretano, V., Littler, K., Lourens, L. J., Lyle, M., Pälike, H., Röhl, U., Tian, J., Wilkens, R. H., Wilson, P. A., and Zachos, J. C.: An astronomically dated record of Earth's climate and its predictability over the last 66 million years, 369, 1383-1387, doi:10.1126/science.aba6853, 2020.

Yin, Q., and Berger, A.: Individual contribution of insolation and CO2 to the interglacial climates of the past 800,000 years, Climate Dynamics, 38, 709-724, 10.1007/s00382-011-1013-5, 2012.

Yin, Q.: Insolation-induced mid-Brunhes transition in Southern Ocean ventilation and deep-ocean temperature, Nature, 494, 222-225, 10.1038/nature11790, 2013.

Zhang, Z., Zhang, Z., Zhang, Z., Tan, N., He, Z., Huang, C., and Guo, Z.: Resolving Cenozoic climate pattern debate in East Asia: Insights from orbital-scale oscillations, Global and Planetary Change, 232, 104346, https://doi.org/10.1016/j.gloplacha.2023.104346, 2024.

Zheng, W., Yu, Y., Luan, Y., Zhao, S., He, B., Dong, L., Song, M., Lin, P., and Liu, H.: CAS-FGOALS Datasets for the Two Interglacial Epochs of the Holocene and the Last Interglacial in PMIP4, Advances in Atmospheric Sciences, 37, 1034-1044, 10.1007/s00376-020-9290-8, 2020.